Journal of Solid State Chemistry 183 (2010) 2763–2769

Contents lists available at ScienceDirect

Journal of Solid State Chemistry

journal homepage: www.elsevier.com/locate/jssc

Synthesis and crystal structure of a new open-framework iron phosphate $(NH_4)_4Fe_3(OH)_2F_2[H_3(PO_4)_4]$: Novel linear trimer of corner-sharing Fe(III) octahedra

Jin-Xiao Mi [a,*], Cheng-Xin Wang [a], Ning Chen [b,c], Rong Li [a,c], Yuanming Pan [c]

[a] Department of Materials Science and Engineering, College of Materials, Xiamen University, Xiamen 361005, People's Republic of China
[b] Canadian Light Source, University of Saskatchewan, Saskatoon, SK, Canada S7N 0X4
[c] Department of Geological Sciences, University of Saskatchewan, Saskatoon, SK, Canada S7N 5E2

ARTICLE INFO

Article history:
Received 6 June 2010
Received in revised form
26 August 2010
Accepted 5 September 2010
Available online 15 September 2010

Keywords:
Isolated linear trimer
Iron phosphate
Crystal structure
Hydrothermal synthesis
Magnetic properties
XANES Fe *K*-edge

ABSTRACT

A new iron phosphate $(NH_4)_4Fe_3(OH)_2F_2[H_3(PO_4)_4]$ has been synthesized hydrothermally at HF concentrations from 0.5 to 1.2 mL. Single-crystal X-ray diffraction analysis reveals its three-dimensional open-framework structure (monoclinic, space group $P2_1/n$ (No. 14), $a=6.2614(13)$ Å, $b=9.844(2)$ Å, $c=14.271(3)$ Å, $\beta=92.11(1)^\circ$, $V=879.0(3)$ Å^3). This structure is built from isolated linear trimers of corner-sharing Fe(III) octahedra, which are linked by (PO_4) groups to form ten-membered-ring channels along [1 0 0]. This isolated, linear trimer of corner-sharing Fe(III) octahedra, $[(FeO_4)_3(OH)_2F_2]$, is new and adds to the diverse linkages of Fe polyhedra as secondary building units in iron phosphates. The trivalent iron at octahedral sites for the title compound has been confirmed by synchrotron Fe *K*-edge XANES spectra and magnetic measurements. Magnetic measurements also show that this compound exhibit a strong antiferromagnetic exchange below $T_N=17$ K, consistent with superexchange interactions expected for the linear trimer of ferric octahedra with the Fe–F–Fe angle of 132.5°.

1. Introduction

Since the pioneering works of Wilson et al. [1] and Moore and Shen [2] on synthetic aluminophosphates and natural cacoxenite, respectively, enormous efforts and progresses have been made in the synthesis and characterization of phosphates with open-framework structures [3–9]. Phosphates of open-framework structures, similar to other porous materials such as zeolites, are interesting because of their wide industrial and environmental applications ranging from catalysis, ion-exchange, sensing, separation, and immobilization and removal of contaminants [3,7].

Among them, iron phosphates [10–12] are particularly attractive not only because of their rich crystal chemistry but also due to interesting and variable magnetic properties related to diverse linkages of Fe polyhedra [7,13,14]. For example, Maspoch et al. [7] classified iron phosphates into four groups according to the linkage of Fe polyhedra: (1) isolated octahedral iron units; (2) connected Fe–X–Fe clusters; (3) connected Fe–X–Fe chains; and (4) connected Fe–X–Fe layers. Similarly, Riou-Cavellec et al. [14] emphasized the roles of these clusters or secondary building units (SBU) in the solutions in the quest for synthesizing new open-framework materials.

In this contribution, we report the hydrothermal synthesis, synchrotron X-ray absorption near edge structure (XANES) spectroscopy, single-crystal X-ray structure analysis and superconducting quantum interference devices (SQUID) magnetic measurements of a new open-framework iron phosphate. Specifically, XANES and SQUID analyses are used to determine the oxidation state of Fe in the title compound and to measure the magnetic properties of the title compound, respectively. Single-crystal X-ray structure analysis shows that the open-framework structure of the title compound is built from a novel isolated, linear trimer of corner-sharing Fe(III) octahedra. Also, factors on the formation and stability of this isolated linear trimer are discussed by comparison with other polymeric clusters in both natural and synthetic phosphates.

2. Experimental details

2.1. Hydrothermal synthesis

The title compound was synthesized from a mixture of 2.00 g $FeCl_3$ (11.5 mmol), 1.15 g $(NH_4)H_2PO_4$ (10 mmol) and 0.8 mL HF (40%, 18.2 mmol) with a Fe:NH_4:P:F molar ratio of 1.2:1:1:1.8.

* Corresponding author. Fax: +86 5922183937.
E-mail address: jxmi@xmu.edu.cn (J.-X. Mi).

0022-4596/$ - see front matter © 2010 Elsevier Inc. All rights reserved.
doi:10.1016/j.jssc.2010.09.008

After adding 10 mL deionized water, this mixture was transferred into a 30 mL Teflon-lined stainless-steel autoclave, heated stepwise to 110, 120, and 130 °C and held there for 24, 24, and 72 h, respectively, and finally cooled down to room temperature. All starting reagents were of analytical grade and used without any further purification. Solid products of synthesis experiments were washed with deionized water and dried in desiccators.

Table 1
Crystal data and structure refinement of $(NH_4)_4Fe_3(OH)_2F_2[H_3(PO_4)_4]$.

Formula sum	$H_{21}F_2Fe_3N_4O_{18}P_4$
Crystal size (mm^3), color	$0.21\times0.06\times0.06$, pale pink-gray
Formula weight, Z	694.64 g/mol, 2
Crystal system, space-group	Monoclinic, $P2_1/n$(No.14)
Cell parameters (Å, deg.)	a=6.2614(13), b=9.844(2), c=14.271(3), β=92.11(1)
Cell ratio	a/b=0.6361, b/c=0.6898, c/a=2.2792
Cell volume, Calc. density	879.0(3) $Å^3$, 2.624 g/cm^3
Radiation (Å), temperature (K)	Mo$K\alpha$(0.71073, graphite), 293(2)
μ (mm^{-1}), F(0 0 0), $2\theta_{max}$(deg.)	2.933, 698, 56.5
Miller-index-range	$-8\le h\le 8,\ -12\le k\le 13,\ -18\le l\le 18$
R_{int}, $R_{\sigma(I)}$	0.0406, 0.0313
Goodness, N_{para}	1.206, 142
R_{gt} (No.), wR_{all}(No.)	0.0553 (2063), 0.1354 (2119)
LDPH[a],Pearson code	0.990, −0.679, *mP*62
SDABD	Fe–O(F)=0.003, P–O=0.004

[a] LDPH denotes the largest difference electron-density peak / hole (e/$Å^3$). SDABD is the standard deviation of average bond distances.

Table 2
Atomic coordinates and isotropic displacement parameters of $(NH_4)_4Fe_3(OH)_2F_2[H_3(PO_4)_4]$.

Atom	Wyck.	*x/a*	*y/b*	*z/c*	U [$Å^2$]
Fe(1)	4*e*	0.7918(1)	0.70751(6)	0.37850(4)	0.00819(19)
Fe(2)	2*b*	1.00000	1.00000	1/2	0.0090(2)
P(1)	4*e*	0.61415(19)	0.49547(12)	0.21980(8)	0.0101(3)
P(2)	4*e*	0.28690(18)	0.75710(13)	0.43055(8)	0.0111(3)
F(1)	4*e*	0.8246(4)	0.8383(3)	0.48235(19)	0.0132(6)
O(1)	4*e*	0.6746(6)	0.3490(4)	0.2138(2)	0.0176(7)
O(2)	4*e*	0.5874(6)	0.5642(4)	0.1259(2)	0.0153(7)
O(3)	4*e*	0.7775(5)	0.5712(4)	0.2806(2)	0.0145(7)
O(4)	4*e*	0.1033(5)	0.6809(4)	0.3851(3)	0.0185(8)
O(5)	4*e*	0.2438(5)	0.9058(4)	0.4445(3)	0.0156(7)
O(6)	4*e*	0.4796(5)	0.7341(4)	0.3722(2)	0.0155(7)
OH(1)	4*e*	0.3976(6)	0.5001(4)	0.2707(3)	0.0212(8)
OH(2)	4*e*	0.3263(6)	0.6926(4)	0.5300(3)	0.0203(8)
OH(3)	4*e*	0.7591(6)	0.5692(3)	0.4757(2)	0.0157(7)
N(1)	4*e*	0.0654(7)	0.3452(5)	0.3561(3)	0.0219(9)
N(2)	4*e*	0.0812(7)	0.6581(5)	0.1467(3)	0.0230(10)

2.2. Characterization

Powder X-ray diffraction (PXRD) patterns of the title compound were collected on a Phillips Panalytical X-pert diffractometer using Cu $K\alpha_1$ radiation (λ=1.54056 Å) at 40 kV and 30 mA, monochromatized by a secondary graphite monochromator. Single-crystal X-ray diffraction data were collected on a Bruker AXS CCD diffractometer (Mo$K\alpha$ radiation, graphite monochromator, 50 kV/40 mA, scan types: 4 blocks for φ=0°, 90°, 180°, 270°, and $\Delta\omega$=0.3°, 600 frames). The raw X-ray diffraction data were corrected for Lorentz and polarization effects. The crystal structure was solved by direct methods and refined by the full-matrix least-squares method using the SHELXS-97 and SHELXL-97 software packages [15]. Hydrogen atom positions were not determined. The final refinement of 142 parameters led to $R1$=0.055 (for 2063 $I>2\sigma(I)$ unique reflections), w$R2$=0.135 (for all diffraction data, 2119) and S=1.206. The crystal data and refinement results, atomic coordinates and equivalent displacement, anisotropic displacement parameters, and selected interatomic distances and angles, as well as bond valence sums (Σs) of the title compound, $(NH_4)_4Fe_3(OH)_2F_2[H_3(PO_4)_4]$ are listed in Tables 1–5. Further details of the crystal structure investigation are available from the Fachinformationszentrum Karlsruhe, D-76344 Eggenstein—Leopoldshafen (Germany), on quoting the depository number CSD-421526, the name of the authors, and citation of the paper. Fourier transform infrared (FT-IR) spectrum of the title compound (2 mg mixed with 200 mg KBr) was measured on a Nicolet Avatar 360 FT-IR spectrometer with a spectral resolution of 2 cm^{-1}. Semi-quantitative chemical analysis was carried out on an Oxford Instruments Energy Dispersive Spectrometer (EDS).

Magnetic property measurements of the title compound were performed for various magnetic fields between 100 Oe and 10 kOe in the temperature range from 1.9 to 400 K, using a Quantum Design MPMS XL-7 SQUID magnetometer, with a resolution of 5×10^{-8} emu. 72.65 mg of sample was contained in a pre-calibrated silica tube for measurements.

Room-temperature Fe *K*-edge XANES spectra were measured by using the superconducting wiggler sourced (1.9 T) beamline Hard X-ray Micro-Analysis (HXMA) at the Canadian Light source,

Table 3
Anisotropic displacement parameters (in $Å^2$) of $(NH_4)_4Fe_3(OH)_2F_2[H_3(PO_4)_4]$.

Atom	U_{11}	U_{22}	U_{33}	U_{12}	U_{13}	U_{23}
Fe(1)	0.0062(3)	0.0080(3)	0.0104(3)	−0.0005(2)	0.0002(2)	−0.0009(2)
Fe(2)	0.0089(4)	0.0077(4)	0.0105(4)	−0.0007(3)	0.0009(3)	−0.0017(3)
P(1)	0.0100(5)	0.0101(6)	0.0102(5)	−0.0004(4)	0.0005(4)	−0.0021(4)
P(2)	0.0057(5)	0.0134(6)	0.0141(6)	0.0020(4)	0.0005(4)	−0.0021(4)
F(1)	0.0146(13)	0.0137(13)	0.0114(13)	−0.0048(11)	0.0028(10)	−0.004(1)
O(1)	0.0241(19)	0.0139(17)	0.0146(17)	0.0024(14)	0.0007(14)	−0.0011(14)
O(2)	0.0214(18)	0.0120(16)	0.0123(16)	−0.0005(13)	−0.0017(13)	−0.0008(13)
O(3)	0.0134(16)	0.0147(16)	0.0153(16)	−0.0013(13)	−0.0005(13)	−0.0061(13)
O(4)	0.0068(15)	0.0156(17)	0.033(2)	0.0007(13)	−0.0003(14)	−0.0099(15)
O(5)	0.0106(15)	0.0147(17)	0.0219(18)	0.0004(13)	0.0047(13)	−0.0054(14)
O(6)	0.0053(15)	0.0222(18)	0.0192(17)	0.0026(13)	0.0018(13)	−0.0042(14)
OH(1)	0.0143(18)	0.026(2)	0.0237(19)	−0.0032(14)	0.0075(15)	−0.0066(15)
OH(2)	0.0231(19)	0.0223(19)	0.0153(17)	0.0046(15)	0.0000(14)	0.0032(14)
OH(3)	0.0198(17)	0.0103(16)	0.0170(17)	−0.0032(13)	0.0020(14)	0.0081(13)
N(1)	0.022(2)	0.022(2)	0.022(2)	0.0015(18)	−0.0036(18)	0.0052(19)
N(2)	0.013(2)	0.034(3)	0.022(2)	0.0045(19)	0.0051(17)	0.009(2)

Table 4
Selected geometric information of $(NH_4)_4Fe_3(OH)_2F_2[H_3(PO_4)_4]$.

Atoms 1,2	*d* 1,2 [Å]	Atoms 1,2	*d* 1,2 [Å]	Atoms 1,2,3	Angle 1,2,3 [°]
Fe(1)–O(1)^{i}	1.934(4)	[N(1)H$_4$]–OH(3)^{iii}	2.736(6)	O(1)–P(1)–O(2)	113.8(2)
Fe(1)–O(3)	1.937(3)	[N(1)H$_4$]–OH(1)	2.885(6)	O(1)–P(1)–O(3)	109.9(2)
Fe(1)–OH(3)	1.960(3)	[N(1)H$_4$]^{iv}–O(2)	2.941(6)	O(2)–P(1)–O(3)	109.9(2)
Fe(1)–O(4)^{ii}	1.967(3)	[N(1)H$_4$]^{iii}–F(1)	2.989(6)	O(1)–P(1)–OH(1)	106.3(2)
Fe(1)–F(1)	1.968(3)	[N(1)H$_4$]–OH(2)^{x}	3.014(6)	O(2)–P(1)–OH(1)	109.3(2)
Fe(1)–O(6)	1.971(3)	[N(1)H$_4$]–O(3)^{xi}	3.036(6)	O(3)–P(1)–OH(1)	107.4(2)
Fe(2)–F(1)	1.945(3)	[N(1)H$_4$]–O(1)^{xi}	3.123(6)	O(4)–P(2)–O(5)	113.9(2)
Fe(2)–F(1)^{v}	1.945(3)	[N(1)H$_4$]–O(4)	3.338(6)	O(4)–P(2)–O(6)	107.6(2)
Fe(2)–O(2)^{vi}	1.964(3)	[N(1)H$_4$]–OH(3)^{xi}	3.420(6)	O(5)–P(2)–O(6)	111.7(2)
Fe(2)–O(2)^{i}	1.964(3)	[N(1)H$_4$]–O(6)^{ix}	3.439(6)	O(4)–P(2)–OH(2)	106.4(2)
Fe(2)–O(5)^{vii}	1.977(3)	[N(2)H$_4$]–OH(2)^{xii}	2.700(6)	O(5)–P(2)–OH(2)	107.3(2)
Fe(2)–O(5)^{ii}	1.977(3)	[N(2)H$_4$]–F(1)^{xii}	2.844(5)	O(6)–P(2)–OH(2)	109.7(2)
P(1)–O(1)	1.494(4)	[N(2)H$_4$]–O(3)^{xi}	2.875(6)	Fe(2)–F(1)–Fe(1)	132.50(15)
P(1)–O(2)	1.505(4)	[N(2)H$_4$]–O(5)^{ix}	3.028(6)	P(1)–O(1)–Fe(1)^{viii}	140.2(2)
P(1)–O(3)	1.513(3)	[N(2)H$_4$]–OH(1)	3.035(6)	P(1)–O(2)–Fe(2)^{viii}	133.5(2)
P(1)–OH(1)	1.562(4)	[N(2)H$_4$]–O(1)^{iv}	3.209(6)	P(1)–O(3)–Fe(1)	140.1(2)
P(2)–O(4)	1.500(4)	[N(2)H$_4$]–O(2)^{xi}	3.230(6)	P(2)–O(4)–Fe(1)^{xi}	134.2(2)
P(2)–O(5)	1.503(4)	[N(2)H$_4$]–O(2)	3.325(6)	P(2)–O(5)–Fe(2)^{xi}	130.9(2)
P(2)–O(6)	1.508(3)	[N(2)H$_4$]–O(4)	3.406(6)	P(2)–O(6)–Fe(1)	143.8(2)
P(2)–OH(2)	1.566(4)			Fe(1)–Fe(2)–Fe(1)	180.0

(i) $1.5-x, 0.5+y, 0.5-z$; (ii) $1+x, y, z$; (iii) $1-x, 1-y, 1-z$; (iv) $0.5-x, 0.5+y, 0.5-z$; (v) $2-x, 2-y, 1-z$; (vi) $0.5+x, 1.5-y, 0.5+z$; (vii) $1-x, 2-y, 1-z$; (viii) $1.5-x, -0.5+y, 0.5-z$; (ix) $0.5-x, -0.5+y, 0.5-z$; (x) $-x, 1-y, 1-z$; (xi) $-1+x, y, z$; (xii) $-0.5+x, 1.5-y, -0.5+z$.

Table 5
Bond valence sum (Σs) of $(NH_4)_4Fe_3(OH)_2F_2[H_3(PO_4)_4]$.

Atom	Fe(1)	Fe(2)	P(1)	P(2)	N(1)H$_4$	N(2)H$_4$	CN[a]	BV
F(1)	1/1	2/1	–	–	1/1	1/1	4	1.186
O(1)	1/1	–	1/1	–	1/1	1/1	4	2.145
O(2)	–	2/1	1/1	–	1/1	2/2	5	2.169
O(3)	1/1	–	1/1	–	1/1	1/1	4	2.208
O(4)	1/1	–	–	1/1	1/1	1/1	4	1.993
O(5)	–	2/1	–	1/1	–	1/1	3	1.995
O(6)	1/1	–	–	1/1	1/1	/	3	1.902
OH(1)	–	–	1/1	–	1/1	1/1	3	1.428
OH(2)	–	–	–	1/1	1/1	1/1	3	1.542
OH(3)	1/1	–	–	–	2/2	/	3	0.902
CN[a]	6	6	4	4	10	9		
ABD[a]	1.956	1.962	1.518	1.519	3.092	3.073		
BV[a]	3.404	3.213	5.052	5.043	1.248	1.151		

[a] CN: coordination number; ABD: average bond distance; BV: bond valence. The bond valences of NH_4 were calculated on assuming their radius the same as rubidium's. 3.404 vs 3.187 for Fe(1) and 3.213 vs 3.014 for Fe(2) are obtained, respectively, using ferric and ferrous bond-valence parameters.

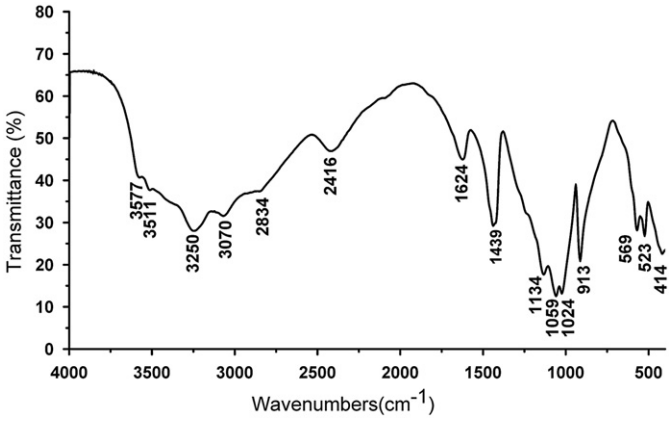

Fig. 1. Fourier transform infrared (FT-IR) spectrum of $(NH_4)_4Fe_3(OH)_2F_2[H_3(PO_4)_4]$.

Saskatoon, Canada. The facility storage ring was running at 2.9 GeV and 250 mA operation mode. During the experiment HXMA was running under mirror-mono-mirror configuration with a Pt strip in the beam path for both collimating and toroidal mirrors. Si(2 2 0) monochromator crystals were used for data collection with primary slits set at 1.0 mm vertical opening width. The monochromator photon energy was calibrated before the data collection, and further in-step calibrated during the experiment at Fe *K*-edge energy (7110.75 eV) [16] using iron metallic foil, and tracked with a Haidenhein rotary encoder attached to the monochromator Bragg rotation axis. XANES data were collected for three reference materials (i.e., natural olivine $(Mg,Fe)_2SiO_4$ and hematite Fe_2O_3 as standards for Fe^{2+} and Fe^{3+}, respectively, and metallic iron foil). The scan step-sizes used were 10 eV/step, 0.25 eV/step, and 0.1 Å^{-1}/step for the pre-edge, XANES and the post edge regions, respectively. Three datasets were collected for each sample, and measurements were performed in the transmission mode for the three reference materials by using straight ion chamber detectors filled with 100% N_2 gas, and in the fluorescence mode with Ge solid state detector for the title compound. The data reduction of the Fe *K*-edge XANES spectra and the least-squares decomposition for the pre-edge multiplet were performed by using WINXAS version 2.3 [17].

3. Structure description

3.1. Description of the title compound

Optical microscopic and scanning electron microscopic examinations show that the title compound is pale pink in color and has a long prismatic morphology (see ESI Fig. 1). The title compound commonly occurs in a matrix with impurity phases such as $FePO_4 \cdot 2H_2O$ or $(NH_4)Fe(HPO_4)_2$, which have been confirmed by measured PXRD patterns (see ESI Fig. 2). Attempts of different starting mixtures and variable experimental conditions to enhance the yield of the title compound were not successful, but did show that this compound can be synthesized from a wide range of HF (40%) concentrations from 0.5 to 1.2 mL. Pure samples of single crystals, used for EDS, FT-IR, XANES and SQUID measurements in this study, were carefully selected by using an optical microscope.

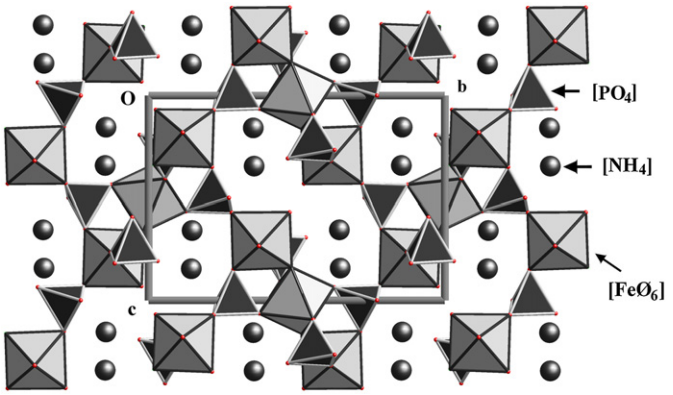

Fig. 2. Three-dimensional open-framework structure of $(NH_4)_4Fe_3(OH)_2F_2[H_3(PO_4)_4]$.

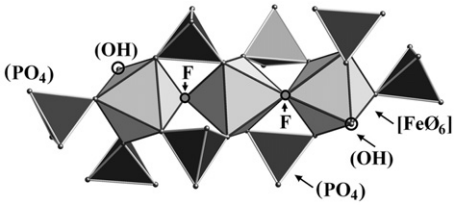

Fig. 3. Linear trimer of $[Fe_3\Phi_{16}]$(Φ: anionic ligands) of $(NH_4)_4Fe_3(OH)_2F_2[H_3(PO_4)_4]$.

The FT-IR spectrum of the title compound (Fig. 1) is interpreted as follows: 3250 and 1439 cm^{-1} due to v_3 and v_4 of $[NH_4]^+$, respectively; 3070 and 1624 cm^{-1} to v_1 and v_2 of $[NH_4]^+$ (activated forbidden modes); 1134, 1059 and 1024 cm^{-1} to v_3 of $[PO_4]^{3-}$; 569 and 523 cm^{-1} to v_4 of $[PO_4]^{3-}$; 913 cm^{-1} to νP–OH; 3577, 3511, 2834 and 2416 cm^{-1} to νOH^- or OH···O [18–20]. Semi-quantitative EDS analyses yielded an average F:Fe:P atomic ratio of ~2:3:4 (see ESI Fig. 3). This ratio has been confirmed by single-crystal X-ray structure refinements that gave a formula $(NH_4)_4Fe_3(OH)_2F_2[H_3(PO_4)_4]$ (see below).

3.2. Crystal structure

The most salient feature of the title compound $(NH_4)_4Fe_3(OH)_2F_2[H_3(PO_4)_4]$ is its three-dimensional open-framework structure that is built from linear trimers of Fe(III) octahedra linked by PO_4 tetrahedra (Fig. 2). Iron atoms occur at two crystallographically distinct positions: Fe(1) and Fe(2) at Wyckoff 4*e* and 2*b* sites, respectively. The iron-based trimers consist of two $[Fe(1)FO_4(OH)]$ octahedra on the sides linked by two trans F-vertices to a central $[Fe(2)F_2O_4]$ octahedron (Fig. 3), hence a Fe–F–Fe–F–Fe configuration with the Fe–F–Fe and Fe–Fe–Fe angles of 132.5° and 180°, respectively. The $[Fe(2)F_2O_4]$ octahedron shares corners with four (PO_4) groups. Similarly, each $[Fe(1)FO_4(OH)]$ octahedron shares corners with four (PO_4) groups but has one terminal OH group, which is indicated by bond valance calculations (Table 5). Bond valence calculations also show that both Fe(1) and Fe(2) are occupied by trivalent Fe (Table 5), which is supported by results from both magnetic measurements and Fe *K*-edge XANES spectra (see below). Other lines of evidence for trivalent iron in the title compound include: (1) the use of $FeCl_3$ as the starting material, (2) absence of any reducing agent, and (3) stability of Fe^{3+} on the basis of redox calculations at the experimental conditions.

Phosphorous atoms also occur at two crystallographically distinct positions and are both coordinated to four oxygen atoms. Both of these two (PO_4) groups have three regular P–O bonds from 1.494(4) to 1.513(3) Å, but a forth, considerably longer P–O bond of 1.562(4) and 1.566(4) Å each (Table 4). The oxygen atoms of the regular P–O bonds are shared with a neighboring iron octahedron each. The considerably longer P–O bond suggests that these oxygen atoms belong to the hydroxyl groups (OH(1) and OH(2); Table 5). Also, the [N(1)H4]–OH(1) and [N(2)H4]–OH(2) distances are ~0.1 Å shorter than the polyhedral average, suggesting that OH(1) and OH(2) are $[(OH)_{3/4}O_{1/4}]$. Similarly, Moore and Araki [21] on electrostatic grounds interpreted that OH(3) in synthetic $(NH_4)H_8Fe_3(PO_4)_6\cdot 6H_2O=[(OH)_{2/3}O_{1/3}]$ is statistically distributed.

The linkage of each Fe(III) octahedral trimer with the (PO_4) groups to form a cluster of $\{Fe_3(HO)_2F_2[H_3(PO_4)_4]\}^{4-}$. These ferric trimeric clusters are oriented along two directions, extending nearly perpendicular to (287) or $(2\bar{8}7)$. Two pairs of differently oriented clusters are interconnected via (PO_4) groups to form a ten-membered-ring (*OTOOTOTOOT*) channel along [1 0 0], in which the NH_4^+ ions reside. The channel with a dimension of ~12 Å × 3.5 Å can be envisaged by the above ferric trimeric clusters connected by isolated (PO_4) groups via sharing O-vertices to form the three-dimensional open-framework structure.

3.3. Magnetic properties

Fig. 4 shows the thermal evolution of inverse magnetic susceptibility (χ^{-1}) in the temperature range from 1.9 to 400 K. It is characteristic of an antiferromagnet below $T_N=17$ K. Above ~50 K, the magnetic susceptibility values match the Curie–Weiss law:

$$\chi(T) = C/(T-\theta_P),$$

yielding $C=4.27$ emu K mol^{-1}[$\mu_{eff}=\sqrt{(8C)}=5.85$ μB per Fe] and the asymptotic Curie temperature $\theta_P=-187$ K. The calculated effective magnetic moment of 5.85 μB is close to the theoretically expected value of 5.9 μ_B for high-spin ferric iron, hence providing further support for the presence of Fe(III) as suggested by bond valence calculations (Table 5). The asymptotic Curie temperature is indicative of strong antiferromagnetic interactions, consistent with strong superexchange interactions expected for the Fe–F–Fe angle of 132.5°.

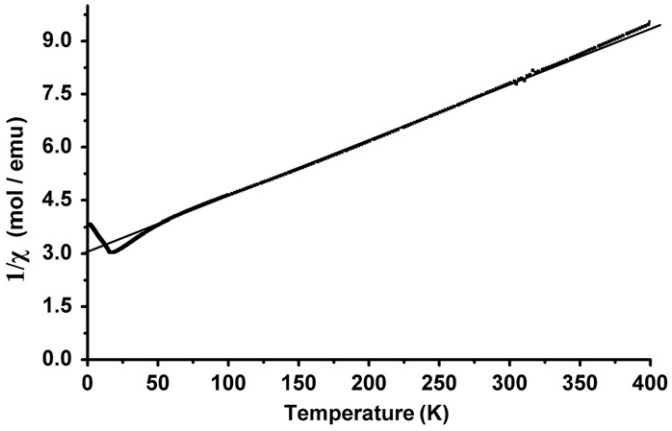

Fig. 4. Magnetic profile of $(NH_4)_4Fe_3(OH)_2F_2[H_3(PO_4)_4]$.

3.4. Fe K-edge XANES spectra

Fig. 5a shows that the main absorption edge of the Fe *K*-edge XANES spectrum of the title compound is closely comparable to that of hematite but distinct from that of olivine, suggesting that Fe in the title compound is largely trivalent. This suggestion has been further evaluated by component fittings for the pre-edge multiplet of the XANES spectrum of the title compound, guided by the fitting for the two reference materials olivine and hematite (Fig. 5a). Based on the Z+1 model [22–25], two electronic transitions (i.e., *L*1 and *L*2) are expected from the 1*s* core level between $1s \rightarrow 3d$ for Fe(III) in an octahedral coordination [23,24,26], while non $1s \rightarrow 3d$ transitions have also been reported and are probably attributable to long-range order [27,28]. There is no consensus regarding the number of non $1s \rightarrow 3d$ transitions involved in the curve fitting for the pre-edge feature attributed to the octahedral Fe(III) in different mineral species, varying from 1 line for ferrihydrite and epidote [28,29], 2 lines for akaganeite, goethite and hematite [28,30], and 3 lines for hematite [28,29]. For the title compound, the contribution from the non $1s \rightarrow 3d$ transition is clearly visible on the high-energy side of the background-subtracted pre-edge multiplet (Fig. 5b). Because the pre-edge feature of the title compound has not been investigated previously, we have attempted all three curve-fitting schemes with the number of the non $1s \rightarrow 3d$ lines from 1 to 3. Specifically, the FWHM fitting for *L*1 and *L*2 was correlated, and floated in step following Petit et al. [29] and Wilke et al. [28] by using the pseudo-Voigt profile [23,26,28,29], while the non $1s \rightarrow 3d$ lines were floated individually for FWHM and the lineshape of their pseudo-Voigt profiles as well.

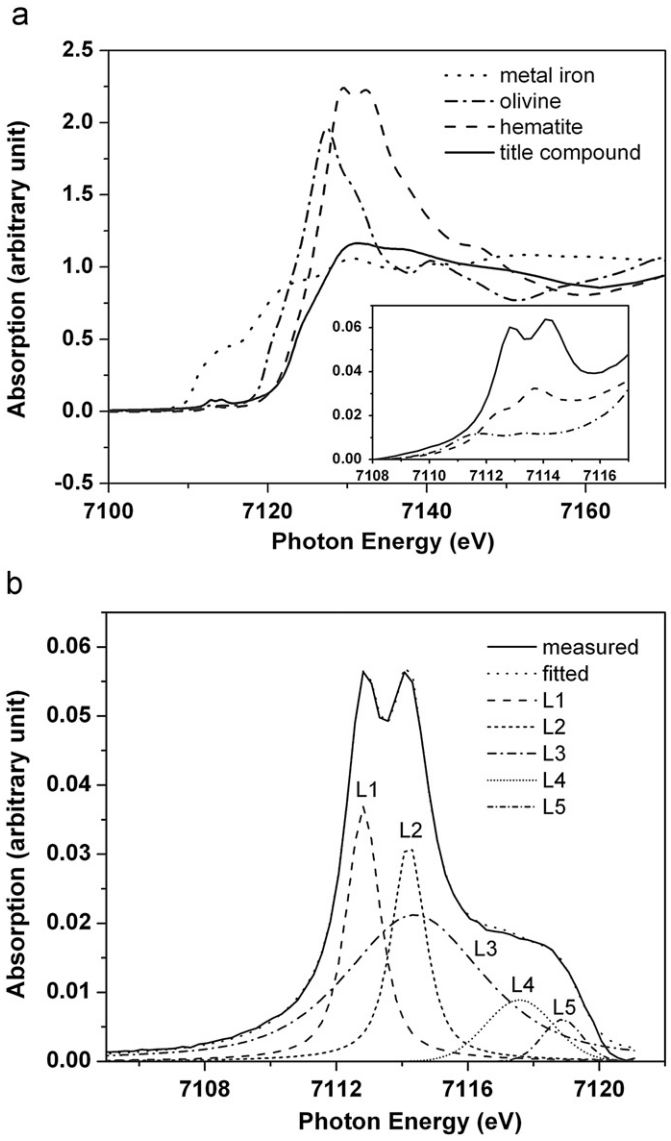

Fig. 5. (a) Fe *K*-edge XANES spectra of the title compound and the three reference materials (metallic iron foil, olivine, and hematite). Inset showing the enlarged pre-edge region of XANES spectra. Note that the vertical scale is identical for the three datasets but offsets have been introduced to match the starting points of the spectra to facilitate direct comparison. (b) Background-subtracted pre-edge multiplet for the title compound and its peak decomposition with pseudo-Voigt profile for the two $1s \rightarrow 3d$ transitions (*L*1 and *L*2) and 3 non $1s \rightarrow 3d$ transitions (*L*3, *L*3 and *L*5).

Fitting results reveal that the number of the non $1s \rightarrow 3d$ lines involved has no apparent impact on either the estimated line positions of *L*1 and *L*2 or the splitting between these two lines, which were then excluded in the calculation for the pre-edge centroid [28,29]. However, significant differences in the relative intensities between *L*1 and *L*2 and between the *L*1 and *L*2 as a whole vs the non $1s \rightarrow 3d$ transitions are apparent among the three schemes. Moreover, significant effect is evident in the lineshape of the $1s \rightarrow 3d$ transition lines. For example, *L*1 and *L*2 have pure Lorentzian lineshape, when 1 or 2 non $1s \rightarrow 3d$ lines are used in fittings. However, the lineshapes of *L*1 and *L*2 are estimated to have 27% Gaussian component, when 3 non $1s \rightarrow 3d$ lines are included. Although Lorentzian profile is expected for electronic transition [24], Gaussian contribution is often convoluted into the lineshape of the experimentally detected pre-edge multiplets owing to the instrumental resolution [23,26,28,29]. Further evidence supporting the fitting scheme with 3 non $1s \rightarrow 3d$ lines is that it yields the smaller fitting residual than its counterparts. Therefore, the fitting results with 3 non $1s \rightarrow 3d$ lines are reported herein (Fig. 5b), with the estimated energy positions of *L*1 (7112.8 eV), *L*2 (7114.2 eV), the centroid (7113.5 eV), and FWHM (1.2 eV). These results are in good agreement with those for octahedral Fe(III) in hematite [28,31], confirming that Fe in the title compound is trivalent with octahedral coordination. The lineshapes of the 3 non $1s \rightarrow 3d$ lines converge to quasi-Gaussian (i.e., 80% Guassian in average), consistent with those reported by Wikle et al. [28] as well.

4. Discussion

Trimers consisting of three mononuclear or polynuclear octahedra, although those involving other similar polyhedra (e.g., trigonal bipyramids and square pyramids) are also included, are common building units in phosphates and are known to exert important influences on the catalytic and magnetic properties of these materials [6,7,14,32,33]. However, most trimers in both natural and synthetic phosphates polymerize further to form larger clusters (e.g., tetramer, pentamer, heptamer, etc.) or infinitely extended chains, columns, layers, and frameworks [7,14,32–34]. There are relatively few examples of isolated trimers linked by (PO_4) groups (Fig. 6). For example, Riou-Cavellec et al. [6] reported an isolated trimer of trans-edge-sharing Fe(II) octahedra [$Fe_3\Phi_{14}$] (Φ: anionic ligands) in [$Fe_3(OH)_2(H_2O)_4(O_3P–(CH_2)_2–CO_2H)_2$] (Fig. 6a). Two more examples of isolated trimers are [$V_3\Phi_{16}$] in [$C_2N_2H_{10}$][$(VO)(VO_2)[V(OH_2)](PO_{3.5})_4 \cdot H_2O$ [35] and [$V^{III}(H_2O)]_3O(O_2CC_6H_4CO_2)_3 \cdot (Cl,9H_2O)$ [36]. The former is composed of three corner-sharing [$V\Phi_6$] octahedra and has a V–V–V angle of 164.5° (Fig. 6b), whereas the latter is built from three [$VO_5(H_2O)$] octahedra sharing one common corner (Fig. 6c). It is

noteworthy that these three compounds with isolated trimers were synthesized from organic templates and contain organic molecules, and none being linear.

To the best of our knowledge, there are only two compounds of inorganic iron phosphates with isolated trimers (Table 6). One is $CsFe_3(PO_4)_3(OH_2)_2$, in which a central $Fe^{(II)}O_4(OH)_2$ octahedron is linked with two $Fe^{(III)}O_5$ bipyramids by *cis*-sharing corners, resulting in a Fe–Fe–Fe angle of 111.8° (Fig. 6d) [5]. Another is $Fe^{II}Fe^{III}_2(P_2O_7)_2$, in which an isolated $[Fe_3\Phi_{12}]$ trimer is built from a central $[Fe^{II}\Phi_6]$ trigonal prism sharing pairs of basal faces with two $[Fe^{III}\Phi_6]$ octahedra on the ends, resulting in a Fe–Fe–Fe angle of 178.3° (Fig. 6e) [37].

Therefore, the isolated, linear trimer of corner-sharing $Fe^{(III)}$ octehedra $[Fe_3\Phi_{16}]$ in the title compound is novel and adds to the diverse linkages of Fe polyhedra as the secondary building units in iron phosphates. We do note that linear trimers of corner-sharing octahedra $[M_3\Phi_{16}]$ have been reported as parts of larger clusters or infinitely extended chains and layers. For example, synthetic $[Me_2NH_2]K_4[(VO)_{10}(H_2O)_2(OH)_4(PO_4)_7]\cdot 4H_2O$ is built from a pentamer $[V_5\Phi_{24}]$, in which the central part involves a linear trimer of corner-sharing $[V\Phi_6]$ octahedra but is linked directly to two $[V\Phi_5]$ square pyramids [38]. Similarly, numerous examples of infinitely extended chains of corner-sharing octahedra, including Fe(III) octahedra, are known to occur in both natural and synthetic phosphates. For example, Moore reported the framework structure of dufrenite to consist of linear corner-sharing octahedral trimers (Fe^{3+}–Fe^{2+}–Fe^{3+}) linked directly to face-sharing octahedral trimers (Fig. 6f) [34].

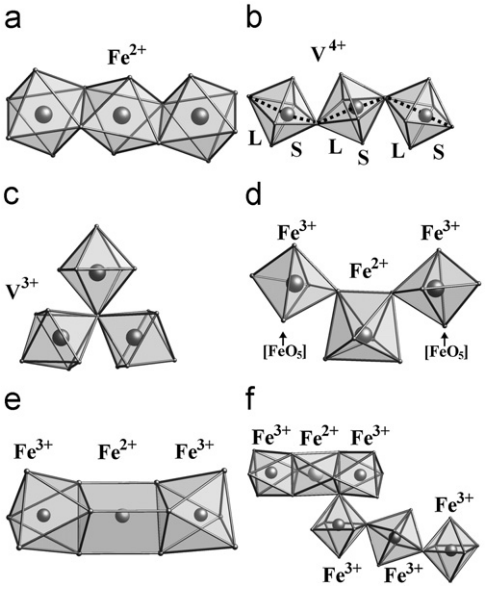

Fig. 6. Illustration of previously reported isolated trimers (a, b, c, d and e), as well as dufrénite (f) with two kinds of non-isolated trimers for comparison. The relationship of octahedra in this paper was defined '*tran-*' as in Fig. 6a, and '*cis-*' as in Fig. 6d. In VO_6 octahedra of Fig. 6b, S and L denote the shorter and longer distances (vs four intermediate ones) of V–O bonds, respectively.

The most salient feature of the isolated linear trimer in the title compound is that the three $[Fe\Phi_6]$ octahedra are linked by two F^- bridging ions. This configuration is similar to those present in a number of F-bearing phosphate minerals. For example, the structure of minyulite $K[Al_2F(H_2O)_4(PO_4)_2]$ possesses dimeric clusters that contain two Al octahedra share one F^- vertex [39,40]. Similarly, the structure of fluellite $Al_2(PO_4)F_2(OH)\cdot 7H_2O$ is composed of F^- corner-sharing chains of Al octahedral [41]. Kampf [39] noted that the perfect electrostatic valence balance is attained when F^- ligates with two trivalent cations, whereas ligation to three trivalent cations would cause severe bond strength over saturation of F^- by 0.5 e.s.u. This situation contrasts the requirements of electrostatic bond valence with other anions such as O^{2-} and OH^-. For example, Kampf [39] pointed out that ligation of OH^- to two trivalent cations results in undersaturation of the anion by 0.17 e.s.u., whereas ligation to three trivalent cations leads to oversaturation by 0.33 e.s.u. This explains the general absence of isolated dimmers and trimers of trivalent cation octahedra with OH^- as the bridging ion. The presence of the isolated linear trimer in the title compound obviously is consistent with the above electrostatic bond valence consideration of Kampf [39]. Our synthesis experiments confirmed that F is required in the formation (and stability) of the title compound. Also, the title compound appears to be stable in a range of F concentrations.

It is also noteworthy that the layer structure of minyulite is linked by K^+ ions, whereas the channels of the title compound are occupied by the $(NH_4)^+$ groups. The effective radius of the $(NH_4)^+$ group is approximately similar to that of Rb^+ [18]. Further synthesis experiments are needed to explore whether larger cations (e.g., Cs^+) or organic groups are capable of stabilizing longer linear clusters (i.e., tetramers) and pentamers of ferric iron octahedra (and those of other trivalent cations) in F-bearing phosphate systems. If yes, these longer linear clusters are expected to lead new open framework phosphates with substantially larger channels.

Table 6
Isolated trimers in iron phosphates.

Trimers	Example	Linkage, shape	Ref.
$[Fe_3\Phi_{12}]$[a]	$Fe^{II}Fe^{III}_2(P_2O_7)_2$	Isolated $[Fe_3\Phi_{12}]$ trimers built from ferrous $[Fe^{II}\Phi_6]$ trigonal prisms sharing pairs of base faces with ferric $[Fe^{III}\Phi_6]$ octahedra (angle of Fe–Fe–Fe = 178.3°)	[37]
$[Fe_3\Phi_{14}]$	$Cs(Fe^{II}Fe^{III}_2(PO_4)_3(H_2O)_2)$	Isolated $[Fe_3\Phi_{14}]$ trimer built from a central ferrous $[Fe^{II}\Phi_6]$ octahedron by sharing its *cis*-vertices with two ferric $[Fe^{III}\Phi_5]$ trigonal bipyramids (angle of Fe–Fe–Fe = 111.8°)	[5]
$[Fe_3\Phi_{14}]$	$[Fe_3(OH)_2(H_2O)_4(O_3P–(CH_2)_2–CO_2H)_2]$	Isolated, *trans*-edge-sharing within trimer (angle of Fe–Fe–Fe = 180.0°)	[6]
$[V_3\Phi_{16}]$[b]	$[V^{III}(H_2O)]_3O(O_2CC_6H_4CO_2)_3\cdot(Cl, 9H_2O)$	Isolated, co-corner-sharing trimer (angle of V–V–V = 60.0°)	[36]
$[V_3\Phi_{16}]$[b]	$[C_2N_2H_{10}]\{(VO)(VO_2)[V(OH_2)](PO_{3.5})_4\}\cdot H_2O$	Isolated $[V_3\Phi_{16}]$ trimer of *trans*-vertices sharing $[V\Phi_6]$ octahedra (angle of V − V − V = 164.5°)	[35]
$[Fe_3\Phi_{16}]$	$(NH_4)_4Fe_3(OH)_2F_2[H_3(PO_4)_4]$	Isolated linear $[Fe_3\Phi_{16}]$ trimer of *trans*-vertices sharing $[Fe\Phi_6]$ octahedra (angle of Fe − Fe − Fe = 180.0°)	This study
$[Fe_3\Phi_{12}]$ & $[Fe_3\Phi_{16}]$ [b]	$Ca(Fe_6(OH)_6(H_2O)_2(P\ O_4)_4)_2$ (dufrénite)	Two kinds of trimers. $[Fe_3\Phi_{12}]$ trimer of an $[Fe^{II}\Phi_6]$ sharing *trans*-faces with two $[Fe^{III}\Phi_6]$ octahedra; $[Fe_3\Phi_{16}]$ trimer of *trans*-vertices sharing $[Fe\Phi_6]$ octahedra.	[34]

[a] Φ denotes anionic ligands as O, F, etc.
[b] Vanadium compounds and non-isolated trimers for comparison.

Acknowledgments

We thank National Natural Science Foundation of China (No. 40972035) and Natural Science and Engineering Research Council of Canada for financial support. The XANES experiment described in this paper was performed at HXMA beamline at the Canadain Light Source, which is supported by NSERC, NRC, CIHR, and the University of Saskatchewan.

Appendix A. Supporting information

Supplementary data associated with this article can be found in the online version at doi:10.1016/j.jssc.2010.09.008.

References

[1] S.T. Wilson, S. Oak, B.M. Lok, E.M. Flanigen, W. Plains, US Patent No. 4310440, 1982.
[2] P.B. Moore, J. Shen, Nature 306 (1983) 356–358.
[3] T.E. Gier, G.D. Stucky, Nature 349 (1991) 508–510.
[4] M. Cavellec, D. Riou, J.M. Greneche, G. Ferey, J. Magn. Magn. Mater. 163 (1996) 173–183.
[5] K.H. Lii, C.Y. Huang, J. Chem. Soc. Dalton 4 (1995) 571–574.
[6] M. Riou-Cavellec, M. Sanselme, M. Nogues, J.M. Greneche, G. Ferey, Solid State Sci. 4 (2002) 619–625.
[7] D. Maspoch, D. Ruiz-Molina, J. Veciana, Chem. Soc. Rev. 36 (2007) 770–818.
[8] S. Natarajan, S. Mandal, Angew. Chem. Int. Edit. 47 (2008) 4798–4828.
[9] S. Natarajan, P. Mahata, Chem. Soc. Rev. 38 (2009) 2304–2318.
[10] K.V. Redrup, M.T. Weller, Dalton Transa. 19 (2009) 3786–3792.
[11] V. Pralong, R. Baies, V. Caignaert, B. Raveau, Inorg. Chem. 48 (2009) 6835–6844.
[12] B. Lajmi, M. Hidouri, A.K. Ben Hammouda, A. Wattiaux, L. Fournes, J. Darriet, M.Ben Amara, Mater. Chem. Phys. 113 (2009) 372–375.
[13] G. Amthauer, G.R. Rossman, Phys. Chem. Miner. 11 (1984) 37–51.
[14] M. Riou-Cavellec, D. Riou, G. Ferey, Inorg. Chim. Acta 291 (1999) 317–325.
[15] G.M. Sheldrick, in: SHELXS-97 and SHELXL-97[CP], University of Göttingen, Göttingen, 1997.
[16] S. Kraft, J. Stümpel, P. Becker, U. Kuetgens, Rev. Sci. Instrum. 67 (1996) 681–687.
[17] T. Ressler, J. Phys. IV. 7 (1997) 269–270.
[18] J.X. Mi, S.M. Luo, H.Y. Sun, X.X. Liu, Z.B. Wei, J. Solid State Chem. 181 (2008) 1723–1730.
[19] A. Hadrich, A. Lautie, T. Mhiri, J. Raman Spectrosc. 31 (2000) 587–593.
[20] A. Hadrich, A. Lautie, T. Mhiri, F. Romain, Vib. Spectrosc. 26 (2001) 51–64.
[21] P.B. Moore, T. Araki, Am. Mineral. 64 (1979) 587–592.
[22] A.J. Berry, H.S. O'Neill, K.D. Jayasuriya, S.J. Campbell, G.J. Foran, Am. Mineral. 88 (2003) 967–977.
[23] L. Galoisy, G. Calas, M.A. Arrio, Chem. Geol. 174 (2001) 307–319.
[24] G. Calas, J. Petiau, Solid State Commun. 48 (1983) 625–629.
[25] G.R. Shulman, Y. Yafet, P. Eisenberger, W.E. Blumberg, Proc. Natl. Acad. Sci. USA 73 (1976) 1384–1388.
[26] T.E. Westre, P. Kennepohl, J.G. DeWitt, B. Hedman, K.O. Hodgson, E.I. Solomon, J. Am. Chem. Soc. 119 (1997) 6297–6314.
[27] G. Dräger, R. Frahm, G. Materlik, O. Brummer, Phys. Status Solidi B 146 (1988) 287–294.
[28] M. Wilke, F. Farges, P.E. Petit, G.E. Brown, F. Martin, Am. Mineral. 86 (2001) 714–730.
[29] P.E. Petit, F. Farges, M. Wilke, V.A. Sole, J. Synchrotron. Radiat 8 (2001) 952–954.
[30] J.M. Combes, A. Manceau, G. Calas, J.Y. Bottero, Geochim. Cosmochim. Acta 53 (1989) 583–594.
[31] F. Di Benedetto, F. D'Acapito, G. Fornaciai, M. Innocenti, G. Montegrossi, L.A. Pardi, S. Tesi, M. Romanelli, Phys. Chem. Miner. 37 (2010) 283–289.
[32] P.B. Moore, S. Ghose, Am. Mineral. 56 (1971) 1527 &.
[33] E. Sokolova, F.C. Hawthorne, Can. Mineral 39 (2001) 1275–1294.
[34] P.B. Moore, Am. Mineral. 55 (1970) 135–169.
[35] L.Y. Duan, M. Yuan, E. Wang, Y.G. Li, Y. Lu, C.W. Hu, J. Mol. Struct. 654 (2003) 95–101.
[36] K. Barthelet, D. Riou, G. Ferey, Chem. Commun. (2002) 1492–1493.
[37] M. Ijjaali, G. Venturini, R. Gerardin, B. Malaman, C. Gleitzer, Eur. J. Solid State Inorg. Chem. 28 (1991) 983–998.
[38] V. Soghomonian, Q. Chen, R.C. Haushalter, J. Zubieta, C.J. Oconnor, Science 259 (1993) 1596–1599.
[39] A.R. Kampf, Am. Mineral. 62 (1977) 256–262.
[40] E. Dumas, F. Taulelle, G. Ferey, Solid State Sci. 3 (2001) 613–621.
[41] B.B. Guy, G.A. Jeffrey, Am. Mineral. 51 (1966) 1579–1592.